



HAL
open science

Pore network geometry in low permeability argillites from magnetic fabric data and oriented mercury injections

Lionel Esteban, Yves Géraud, Jean Luc Bouchez

► **To cite this version:**

Lionel Esteban, Yves Géraud, Jean Luc Bouchez. Pore network geometry in low permeability argillites from magnetic fabric data and oriented mercury injections. *Geophysical Research Letters*, 2006, 33, pp.18311. 10.1029/2006GL026908 . hal-00319750

HAL Id: hal-00319750

<https://hal.science/hal-00319750>

Submitted on 20 May 2021

HAL is a multi-disciplinary open access archive for the deposit and dissemination of scientific research documents, whether they are published or not. The documents may come from teaching and research institutions in France or abroad, or from public or private research centers.

L'archive ouverte pluridisciplinaire **HAL**, est destinée au dépôt et à la diffusion de documents scientifiques de niveau recherche, publiés ou non, émanant des établissements d'enseignement et de recherche français ou étrangers, des laboratoires publics ou privés.

Pore network geometry in low permeability argillites from magnetic fabric data and oriented mercury injections

Lionel Esteban,^{1,2,3} Yves Géraud,² and Jean Luc Bouchez¹

Received 18 May 2006; revised 3 July 2006; accepted 10 July 2006; published 26 September 2006.

[1] The relationship between mineral fabric and pore network geometry anisotropy is studied for representative clay-rich lithologies from the Callovo-Oxfordian formation of the Andra Laboratory (Paris Basin, France), sampled from the oblique borehole-core #EST211. Comparisons between standard magnetic fabric measurements (AMS) that give the mineral fabric, high pressure mercury injections parallel to the AMS axes, that reflect the pore structure parameter and AMS measurement after impregnation with a ferrofluid at different pressures, giving the shape of the pore networks, allow us to propose three pore models. (1) In the silt-enriched specimens the transfer pathway is found to be controlled by vertical pathways. (2) In the carbonate-enriched specimens the best transfer pathway is parallel to bedding, and in this plane is almost isotropic in spite of an anisotropic pore structure. (3) In the clay-enriched specimens, at the site of the Andra Laboratory, the transfer pathway is also parallel to bedding and $\sim 20\%$ higher parallel to both the magnetic lineation and the pore shape preferred orientation. **Citation:** Esteban, L., Y. Géraud, and J. L. Bouchez (2006), Pore network geometry in low permeability argillites from magnetic fabric data and oriented mercury injections, *Geophys. Res. Lett.*, 33, L18311, doi:10.1029/2006GL026908.

1. Introduction

[2] Mudrocks, as major constituents of sedimentary basins, have been proposed to host experimental sites for nuclear waste storage because of their extremely low permeability (down to 10^{-22}m^2 [Neuzil, 1994]) and high sealing ability. These intrinsic properties are controlled by interaction between rock microstructure, chemical interactions between mineral and fluid, and characteristics of permeating fluid [Hildenbrand and Urai, 2003]. Mudrock structure is controlled by the platy nature of the clay minerals that leads to permeability anisotropy, which arises from particle realignment during burial [Al-Tabbaa and Wood, 1987; Dewhurst et al., 1996; Yang and Aplin, 1998]. Horizontal to vertical permeability ratios between 1 to 3 have been measured in clay-rich materials subjected to low levels of stress [Tavenas et al., 1983; Leroueil et al., 1990], but these values are only loosely related to the

porosity. In their model, Yang and Aplin [1998] proposed to take into account a combination of porosity, average alignment of pores, pore shapes and pore throat sizes. They predicted a three-fold increase of the permeability anisotropy due to the decrease of the pore throat size at increasing confining pressure.

[3] The ~ 130 m thick, clay-rich formation of eastern Paris Basin, deposited during the Callovian and beginning of the Oxfordian, has been sampled from the oblique borehole #EST211 of the French radioactive waste management Agency (Andra; Figure 1). It gave us the opportunity to study the textural organization of rocks particularly well preserved from physico-chemical transformations. The anisotropy of magnetic susceptibility (AMS), which provides information on the orientation distribution of the magnetic minerals, is compared to the anisotropy of the pore network obtained by two high-pressure injection methods. The first one consists of mercury injection into three predetermined directions. The second consists of AMS measurements before and after impregnation with a ferrofluid under hydrostatic pressures. We hope to better understand the pore network organization and its relationship with the rock fabric elements. Pore connectivity and permeability anisotropy of shales is a key problem in assessing the reliability of underground storage of nuclear waste.

2. Samples

[4] The argillites under study are dark-coloured, subhorizontal clay-rich laminae finely interfingered with silt-enriching laminae, the whole displaying a very low permeability ($\sim 10^{-20}\text{m}^2$ [Lavanchy and Distinguin, 2005]). 80 cylindrical samples of standard size (height 22 mm; diameter 25 mm), each one integrating a time span of $\sim 1000 \pm 300$ yrs, were collected from the borehole and studied for their pore network geometry. Three representative pairs of specimens from the three main lithologies (15665-A1 & A2, 15610-A1 & A2 and 15348-A1 & A2 in age-order) are presented in detail (Figure 1).

[5] Silt-enriching specimens from lithology 1 (#15665: 518 m) have a notable silt fraction (middle Callovian). Clay-enriched specimens from lithology 3 (#15348: 466 m) are the richest in clay (late Oxfordian). Finally, the carbonate-enriched specimens from lithology 2 (#15610: 510 m; late Callovian), have compositions in-between lithologies 1 and 3 [Gaucher et al., 2004].

3. Techniques

[6] Each specimen was subjected to a preliminary magnetic anisotropy measurement (AMS) using a KLY3 susceptometer (Agico Ltd) that yielded the orientation intensity

¹Laboratoire des Mécanismes et Transferts en Géologie/Centre National de la Recherche Scientifique UMR 5563, Groupement de Recherche en Formation Profonde, UniversitéPaul-Sabatier, Toulouse, France.

²Ecole et Observatoire des Sciences de la Terre/Centre National de la Recherche Scientifique UMR 7516, Groupement de Recherche en Formation Profonde, UniversitéLouis-Pasteur, Strasbourg, France.

³Andra, Châtenay-Malabry, France.

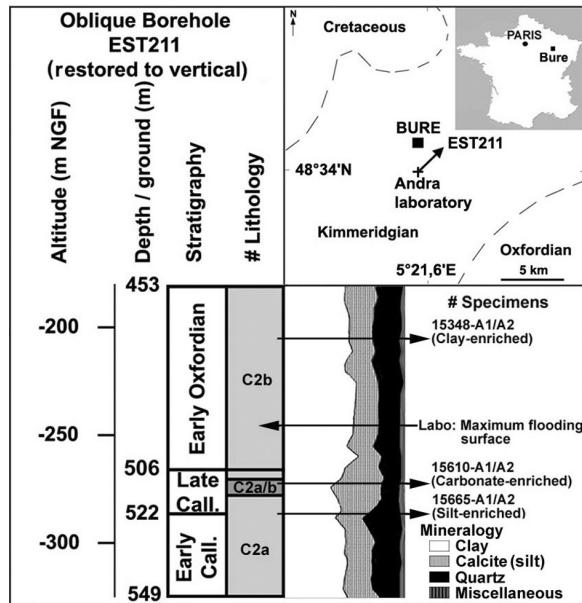


Figure 1. Location of the Andra Laboratory, and log with mineralogy distribution of the oblique drilling from which the three pairs of specimens were collected.

of the principal axes of the susceptibility ellipsoid, $K_1 \geq K_2 \geq K_3$ [Hrouda, 1982]. AMS is a quick non-destructive technique that provides the argillite mineral fabric, mainly carried by the clay minerals [Esteban *et al.*, 2006]. Four parameters characterize the petrofabric: the anisotropy percentage $P\% = ([K_1/K_3] - 1) \times 100$, the planar and linear anisotropies $F\% = ([K_2/K_3] - 1) \times 100$ and $L\% = ([K_1/K_2] - 1) \times 100$, and the shape parameter of Jelinek [1977], $T = [LnF - LnL]/[LnL + LnF]$, comprised between $T = -1$ (prolate) and $T = +1$ (oblate).

[7] The A2 specimens were then cut into parallelepipeds according to the three principal AMS axes. Void volumes and their threshold diameters were measured using mercury injection tests (Micromeritics porosizer, Ltd) that determine the porous network geometry. These tests are based on the principle that a non-wetting fluid penetrates a void if the injection pressure is high enough to overcome capillary forces. For simple void shapes (tubes or cracks), the applied capillary pressure relates to the smallest dimension of the void [Walschburn, 1921], and also depends on the interfacial tension and the mercury wetting angle [Wardlaw and Yu, 1988]. To depict the void geometry along each AMS axis, the A2 specimens were epoxy-coated on sides parallel to the imposed mercury injection direction [Surma *et al.*, 2003] which was applied at increasing pressures up to 300 MPa corresponding to equivalent pore radii of ~ 4 nm. Hg tests provide pore parameters (connected porosity, threshold distribution) that determine the permeability and its variation [Yang and Aplin, 1998].

[8] The A1 specimens were measured for their AMS after ferrofluid impregnation, which gives the anisotropy of the pore network, which can then be compared with the original mineral fabric [Pfleiderer and Halls, 1994]. The ferrofluid used is a non-wetting paraffin oil, that contains a suspension of superparamagnetic particles (~ 15 nm in average size, from Liquids Research Ltd) and surfactant that avoids clustering of the particles. The A1 specimens were impreg-

nated under a progressively increasing hydrostatic pressure (4, 8 and 14 MPa) which allows the fluid to reach pores of decreasing sizes. The pore network fabric given by the magnetic template of the connected porosity is compared with the original mineral fabric by the AMS measurements performed before and after impregnation.

4. Results

[9] The bulk magnetic susceptibility, $K_m = (K_1 + K_2 + K_3)/3$, ranges from 99 μSI for lithos. 1 (silt-enriched) and 2 (carbonate-enriched) to 115 μSI for litho. 3, the richest in clay (Table 1). The anisotropy percentage varies from $P\% = 0.6$ in litho. 2, to 3.2 in lithos. 1 and 3, values which are close to the planar anisotropy, around 0.6 and 2.9 respectively, underlining the high compaction of this material. As expected, the magnetic ellipsoids are highly oblate with T values always larger than 0.7, but it is noticeably less oblate in the carbonate-enriched litho. 2 ($T = 0.7-0.8$) than in the clay- and silt-enriched lithos. 1 and 3 ($T \sim 0.9$; Table 1). In addition, a faint linear anisotropy does exist in the foliation plane, with values as low as 0.05% in lithos. 2 and 3, but reaching 0.16% in litho. 1. After re-orientation with respect to the geographical reference frame (an easy operation in an inclined borehole with a horizontal foliation) this lineation is found to be rather constant within a given lithology, trending mainly NE-SW in the clay-rich litho. 3, and close to N-S in lithos. 2 and 1 [Esteban *et al.*, 2006].

[10] In the silt-enriched specimens (litho. 1) the partial pore volume, measured along each ASM axis, varies by as much as one-third as a function of the orientation, with a maximum ($\sim 13\%$) parallel to K_3 (vertical) and a minimum ($\sim 9\%$) parallel to K_1 (magnetic lineation; Figure 2b). In the carbonate-rich specimens (litho. 2) the partial pore volume varies by about 20%, from more than 8% parallel to K_3 to more than 13% parallel to K_1 (Figure 2c). In the clay-enriched specimens (litho. 3) this pore volume it varies by almost a factor of two, reaching 10% parallel to K_3 and 19% parallel to K_1 (Figure 2d). In the bedding plane, a difference on the order of 20% is measured between K_1 and K_2 in both the silt- and clay-rich lithologies. By contrast, in the carbonate-rich litho. 2, no difference is observed within the bedding plane (Figure 2c). Finally, the pore threshold diameters, given by the pore sizes at the abrupt changes of slope of the saturation curves, are approximately twice as bigger in the clay-enriched litho. 3 (30 nm, Table 1) than in the carbonate- and silt-enriched lithologies (15 nm; Table 1).

[11] The silt-enriched specimens (litho. 1), impregnated with a ferrofluid at low pressure (4 MPa), have the highest values of the pore shape ratios, as measured by $P\%$, flattened almost perpendicular to bedding (Figure 3a and Table 1). At 8 MPa the pores become flattened parallel to bedding and their elongation is parallel to the magnetic lineation of this formation. At the maximum injection pressure (14 MPa) the pore flattening remains parallel to bedding and its elongation trends NE-SW, a direction similar to that of the clay-rich litho. 3 (Figure 3c). In the carbonate-enriched specimens (litho. 2), the pore network is flattened parallel to bedding and its flattening increases with increasing pressure (i.e. with decreasing pore sizes) hence weakening the E-W trending parallel-to-bedding anisotropy (Figure 3b). The clay-enriched specimens (litho. 3) display the highest increase

Table 1. AMS Data for Specimens A1 and A2 Giving Scalar and Directional Parameters (See Text)^a

Specimen	AMS Data										Ferrofuid Injection Data (A1 Specimens)									
	Number	Km, μ SI	Pp %	Lp %	Fp %	T	K1 (Dec°/Inc°)	K3 (Dec°/Inc°)	Hg Injection Axis	Maximum Porosity, %	Mean Threshold Diameter, μ m	Injection Pressure, MPa	Δ Km	Δ Pp	Δ Lp	K1, (Dec°/Inc°)	K3 (Dec°/Inc°)			
15665 Silt-	A1	99	3.1	0.16	2.97	0.9	172/0	233/90	K1	9	0.012	4	3.0	5.3	3.0	141/0	231/31			
	A2	101	3.2	0.13	2.94	0.92	169/1	235/88	K2	11.3	0.017	8	1.0	0.2	0.0	181/1	233/86			
15610 Carb-	A1	103	0.69	0.05	0.64	0.87	215/3	232/84	K3	12.6	0.012	14	1.0	1.1	3.8	248/3	235/87			
	A2	104	0.61	0.09	0.53	0.72	188/5	233/83	K1	13.2	0.012	4	3.5	330.2	180.9	260/2	221/87			
15348 Clay-	A1	114	2.97	0.07	2.9	0.95	214/0	229/88	K2	8.6	0.012	14	1.2	1.2	1.0	275/2	237/88			
	A2	115	2.79	0.06	2.73	0.95	223/0	234/88	K3	15	0.024	4	10.7	5.9	3.1	240/0	236/90			
									18.9	0.033	8	1.0	3.2	1.0	244/1	244/88				
									10.2	0.024	14	1.2	1.5	0.7	231/1	233/89				

^aOriented mercury injection of specimens A2 giving porosities and threshold diameters parallel to the AMS principal directions. Ferrofuid injection data giving variations of the magnetic parameters at 4, 8 and 14 MPa pressures. Δ : normalisation with respect to the previous experimental step.

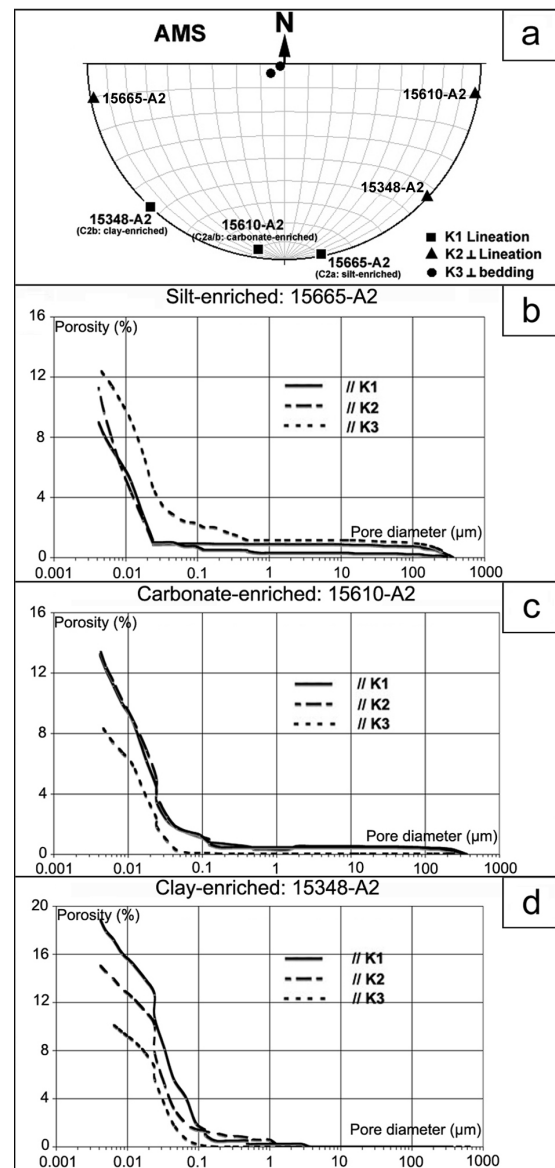


Figure 2. (a) AMS axes (K_1 , K_2 and K_3) in the geographic reference frame of the A2 specimens used for mercury injection. Connected pore volumes (%) versus threshold pore diameters (μ m) measured parallel to the principal magnetic axes: (b) 15665-A2: silt-enriched: highest pore parameters are vertical; (c) 15610-A2: carbonate-enriched: highest pore parameters within the bedding plane, and isotropic in this plane; and (d) 15348-A2: clay-enriched: highest pore parameters within the bedding and anisotropic in this plane.

in susceptibility, hence in connected porosity. Their pore network shows the same shape anisotropy parallel to NE-SW whatever the ferrofluid pressure (Figure 3c). This implies that the pores tend to keep the same shape whatever their sizes, as strengthened by their T values, from 0.95 before ferrofluid injection, to T = 0.74, 0.91 and 0.95 after injection at 4, 8 and 14 MPa respectively.

5. Discussion and Conclusion

[12] Lithology, particle orientations, porosity and pore size distribution do control the permeability and the anisot-

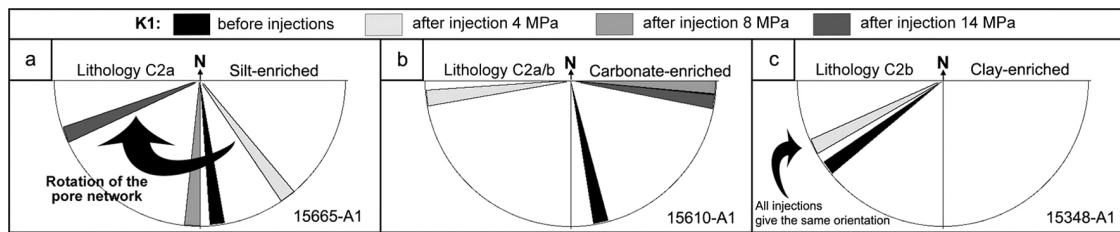


Figure 3. Rose diagrams (oriented with respect to north) of the K_1 magnetic axes (lineation) before (in black) and after impregnation with a ferrofluid at three different pressures (gray-tones) for the A1 specimens. (a) Silt-rich: at 4 MPa the magnetic plane is subvertical (K_3 close to horizontal) but K_1 remains horizontal. (b) Carbonate-rich: K_1 after impregnation is almost perpendicular to lineation before impregnation. (c) Clay-rich: K_1 does not change the impregnation pressure in spite of large variation in magnetic susceptibility.

ropy of mudstones [Yang and Aplin, 1998]. In this study, we document how particle orientation (AMS) and pore parameters, like pore shapes (ferrofluid impregnation) and threshold values (mercury injection), are related. The magnetic fabric before impregnation reflects the mineral organization acquired during deposition and burial, i.e., clay minerals in case of the clay- and carbonate-enriched lithologies, and ferrimagnetic grains (mainly iron oxides) in addition to the clay minerals, for the silt-enriched lithologies. Depending on these lithological characters, three porous models are proposed.

[13] (1) The simplest model is represented by the carbonate-enriched lithology which has the lowest pore parameters in the vertical direction and similar values in the bedding plane. Surprisingly, as measured before ferrofluid injection, void elongations are perpendicular to K_1 . This agrees with the observed orientation of some calcite-filled micro-tension gashes. (2) The second model corresponds to the clay-enriched lithology where a remarkable agreement is observed between particle orientation, void shapes and pore parameters parallel to NE-SW within the bedding plane. In this model, the pore network mimics the mineral fabric and the better pathway is parallel to the lineation. In this lithology, the mineral lineation likely reflects a zone-axis organization of the clay minerals [Housen et al., 1993], giving micro-tubes whose axes are parallel to the currents [Ellwood and Ledbetter, 1979] or to the extension direction to which the sediment was subjected during compaction [Heling, 1970; Herbert, 1993]. (3) The silt-rich lithology has apparently the more complex network, pore sizes and their elongations varying according to the increase of mercury and ferrofluid injection pressures, respectively. At low pressures, the vertical axis has the largest pore diameters, the highest partial pore volume (~13%) and the highest pore shape anisotropy ($P = 17.5\%$ at 4 MPa). At the intermediate ferrofluid pressure (8 MPa) where smaller pores are reached, void elongations and shapes are close to N-S. This direction is parallel to the magnetic lineation measured before impregnation (Figure 3a), itself mainly carried by the silt fraction [Esteban et al., 2006]. At the maximum ferrofluid pressure (14 MPa), the smallest pores are reached and their elongation, NE-SW, is similar to that of the clay-rich lithology. We conclude that this lithology integrates three porous networks. The vertical network of the largest pores is tentatively attributed to dewatering during compaction. The two other networks likely relate to different mineral sizes, since (1) the largest pores

(deduced from AMS after impregnation) are elongate parallel to the silt lineation i.e. N-S (deduced from AMS before impregnation); and (2) the smallest pores are elongate parallel to the lineation measured in the clay-enriched lithology (NE-SW).

[14] In conclusion, high pressure injections using both mercury and a ferrofluid, combined with magnetic measurements help us to reveal the sedimentary conditions recorded by the pore network in very low permeability rocks. We have examined two key parameters, porosity and mineralogical content, that control fluid flow and sealing properties. Slight variations of these parameters may modify the fluid paths and hence influence the long term fluid flow. Our study is a prerequisite in modeling rock permeability, for example through an upscaling approach, from pore scale to core scale [Lock et al., 2004], among others [Matthews et al., 2006].

[15] **Acknowledgments.** L. Esteban thanks the Andra agency for his PhD fellowship. GdR FORPRO (CNRS) is acknowledged for financial support. R. Siqueira is thanked for his support in the rock magnetism laboratory. We also thank D. Lahondes, C. Aurière and H. Rebours for providing the samples from the core-storage, and A. Trouiller, B. Yven and P. Lebon for suggestions. This work is the GdR FORPRO contribution 2005/15A.

References

- Al-Tabbaa, A., and D. M. Wood (1987), Some measurements of the permeability of kaolin, *Geotechnique*, **37**, 499–503.
- Dewhurst, D. N., K. M. Brown, M. B. Clennell, and G. K. Westbrook (1996), A comparison of the fabric and permeability anisotropy of consolidated and sheared silty clay, *Eng. Geol.*, **42**, 253–267.
- Ellwood, B. B., and M. T. Ledbetter (1979), Paleocurrent indicators in deep-sea sediment, *Science*, **203**, 1335–1337.
- Esteban, L., J. L. Bouchez, and A. Trouiller (2006), The Callovo-Oxfordian argillites from Eastern Paris basin: magnetic data and petrofabrics, *C. R. Acad. Sci. Paris*, in press.
- Gaucher, E., C. Robelin, J. M. Matray, G. Négrel, Y. Gros, J. F. Heitz, A. Vinsot, H. Rebours, A. Cassagnabère, and A. Bouchet (2004), Andra underground research laboratory: interpretation of the mineralogical and geochemical data acquired in the Callovian-Oxfordian formation by investigative drilling, *Phys. Chem. Earth*, **29**, 55–77.
- Heling, D. (1970), Micro-fabrics of shales and their rearrangement by compaction, *Sedimentology*, **15**, 247–260.
- Herbert, T. D. (1993), Differential compaction in lithified deep-sea sediments is not evidence for “diagenetic unmixing”, *Sed. Geol.*, **84**(1–4), 115–122.
- Hildenbrand, A., and J. L. Urai (2003), Investigation of the morphology of pore space in mudstones—first results, *Mar. Petrol. Geol.*, **20**, 1185–1200.
- Housen, B. A., C. Richter, and B. A. Van der Pluijm (1993), Composite magnetic anisotropy fabrics: experiments, numerical models and implications for the quantification of rock fabrics, *Tectonophysics*, **220**(1–4), 1–12.

- Hrouda, F. (1982), Magnetic anisotropy of rocks and its application in geology and geophysics, *Geophys. Surv.*, 5, 37–82.
- Jelinek, V. (1977), The statistical theory of measuring anisotropy of magnetic susceptibility of rocks and its application, 88 pp., Geofysika, Brno, Czech Republic.
- Lavanchy, J. M., and M. Distinguin (2005), Determination of hydraulic properties of the Callovo-Oxfordian argillite at the Bure site: Synthesis of the results obtained in deep boreholes using several in-situ investigation techniques, paper presented at Clays in Natural and Engineered Barriers: 2nd International Meeting, Andra, Tours, France.
- Leroueil, S., G. Bouclin, F. Tavenas, L. Bergeron, and P. Rochelle (1990), Permeability anisotropy of natural clays as a function of strain, *Can. Geotech. J.*, 27, 568–579.
- Lock, P. A., X. D. Jiang, and R. W. Zimmerman (2004), Comparison of methods for upscaling permeability from the pore scale to the core scale, *J. Hydraul. Res.*, 42, 3–8.
- Matthews, G. P., C. F. Canonville, and A. K. Moss (2006), Use of a void network model to correlate porosity, mercury porosimetry, thin section, absolute permeability and NMR relaxation time data for sandstone rocks, *Phys. Rev. E*, 73, 031307.
- Neuzil, C. E. (1994), How permeable are clays and shales?, *Water Resour. Res.*, 30, 145–150.
- Pfleiderer, S., and H. C. Halls (1994), Magnetic pore fabric analysis: A rapid method for estimating permeability anisotropy, *Geophys. J. Int.*, 116, 39–45.
- Surma, F., et al. (2003), Microstructures d'un grès affecté par une faille normale: Anisotropie de connectivité et de perméabilité, *Bull. Soc. Géol. France*, 174(3), 295–303.
- Tavenas, F., et al. (1983), The permeability of natural soft clays. Part II: Permeability characteristics, *Can. Geotech. J.*, 20, 645–660.
- Walschburn, E. W. (1921), Note on a method of determining the distribution of pores sizes in a porous material, *Proc. Natl. Acad. Sci. U. S. A.*, 7, 115–116.
- Wardlaw, N. C., and L. Yu (1988), Fluid topology pore size and aspect ratio during imbibition, *Transp. Porous Med.*, 3, 17–34.
- Yang, Y., and A. C. Aplin (1998), Influence of lithology and compaction on the pore size distribution and modelled permeability of some mudstones from the Norwegian margin, *Mar. Petrol. Geol.*, 15, 143–175.

J. L. Bouchez and L. Esteban, LMTG/CNRS UMR 5563, GdR FORPRO, Université Paul-Sabatier, 14 Avenue E. Belin, F-31400 Toulouse, France. (esteban@lmtg.obs-mip.fr)

Y. Géraud, EOST/CNRS UMR 7516, GdR FORPRO, Université Louis-Pasteur, 1 rue Blessig, F-67084 Strasbourg, France.